A fabrication history based strain-fatigue model for prediction of crack initiation in a radial loading wheel

A fabrication history based strain-fatigue model for prediction of crack initiation in a radial loading wheel

Yan Zhao[a,b,*], Mingtu Ma[a], Rongshan Qin[b], Yangchao Ling[a], Guangyao Wang[a], Xinming Wan[a], Hairong Gu[c], Yonggang Liu[c]

[a] *Automotive Light-weight Engineering Technology Center, China Automotive Engineering Research Institute Co. Ltd, Chongqing, 401122, P. R. China.*
[b] *Department of Materials Engineering, The Open University, Milton Keynes, MK7 6AA, United Kingdom*
[c] *Automotive Steel Sheet Research Institute, Ma'anshan Iron and Steel Company, Ma'anshan, 243.21, P. R. China.*
[*] *Corresponding Author: Yan Zhao, email: zhaoyansuli1984@163.com*

Abstract

A strain-based fatigue model concerning fabrication history is applied to predict the fatigue life of a commercial car wheel under radial loads. As the prior conditions, the strain fatigue testing is performed on standard specimen of DP590 and FB540 steels at various fabrication states, including raw materials, pre-strain and pre-strain + bake. Furthermore, the strain distribution of car wheel during its rotation under radial loads is simulated via ANSYS. The fatigue properties mainly determined by crack initiation of car wheels at various fabrication states are predicted via local stress-strain method, in which the scale and surface factors are also taken into account. The radial fatigue testing is carried out and the results are used to validate the present model. The fracture mechanism is analyzed using FEI Nova 400 field emission gun scanning electron microscope.

Keywords: Fatigue prediction, car wheel, fabrication history, radial fatigue testing, local stress-strain method

Nomenclature:

b	fatigue strength exponent
c	fatigue ductility exponent
d	circumference of air ventilation hole
d_e	effective dimension
E	elastic modulus
F_0	maximum radial loading force
h	average depth of the hole
N_f	fatigue life
μ	scale parameter
θ	loading angle
θ_0	angle at maximum load
$\Delta\varepsilon_t/2$	total strain amplitude
$\Delta\varepsilon_e/2$	elastic strain amplitude
$\Delta\varepsilon_p/2$	plastic strain amplitude
σ'_f	fatigue strength coefficient
ε'_f	fatigue ductility coefficient
σ_{-1}	fatigue limit
β_1	surface parameter
σ_m	mean stress

1. Introduction

The fatigue property of automobile wheel is pretty important to its safety service. Radial fatigue testing is the mandatory requirement of automobile wheel before its wide application. It has been demonstrated that simulation is an effective method in wheel production including geometric design, stress analysis, fatigue prediction, etc. An effective model can significantly save the consumption of both cost and time for new product design. Numerical study for predicting the fatigue performance of wheel has been reported in previous literatures [1-6]. The fatigue prediction can be fulfilled via nominal stress (using stress-based fatigue model) and local stress-strain (using strain-based fatigue model) methods. Nominal stress method can represent the fatigue behavior of component in which plastic deformation does not exist. Local stress-strain method can cover both elastic and plastic stages during fatigue process, i.e. it is appropriate to evaluate the effect of either only elastic deformation or both elastic and plastic deformations on final fatigue life. The plastic strain is dominant in the area of very low fatigue life. As the fatigue life increases, the elastic strain tends to be the governing factor. Simultaneously, the effect of plastic strain on fatigue life is approaching 0, which reveals an absolute elastic deformation. The profile of industrial automobile component is usually complicated and some locations are liable to experience plastic deformation due to stress concentration resulted by special geometry, thus local stress-strain method is often applied in the initial design of component as well. Firat et al [7] assessed the fatigue damage of truck wheels on the basis of local stress-strain approach by coupling effective strain, Smith-Watson-Topper [8] and Fatemi-Socie parameters [9] into Manson-Coffin model [10-11]. Wang et al [12] applied linear transient dynamic finite element analysis and local stress-strain approach to the rotation bending fatigue testing of automobile wheel. Those elements near to critical regions were employed to predict the fatigue life of wheel via Neuber's rule [13] and local stress-strain approach. Finally, the prediction was coherent with the testing result. In these years, dual phase (DP) steel is widely applied on automobile because of its high strength and excellent formability. It

has been demonstrated that the manufacturing processes, such as stamping and paint baking, can cause the variation in mechanical properties of DP steel. Le et al [14] studied the effect of pre-strain on the mechanical property of DP600, and the result showed that the yield strength was increased by 73% when 8% strain was loaded. Moreover, Shi et al [15] reported that the ultimate strength of DP steel was increased by about 40 MPa after a typical paint baking cycle. However, these significant variations of mechanical property induced by fabrication have not been considered towards the fatigue prediction of component in the previous models.

In this paper, a strain-based fatigue model concerning the fabrication history of commercial car wheel under radial loads is investigated. The local stress-strain method is employed to predict the fatigue life of car wheel. The key parameters of Manson-Coffin model are calculated according to strain fatigue testing. The scale and surface factors are also taken into account due to the long fatigue life of car wheel. Radial fatigue testing of car wheel is carried out to validate the model. The fracture was analyzed via FEI Nova 400 field emission gun scanning electron microscope (SEM).

2. Experiment

2.1 Fatigue testing of materials

In order to achieve the light weight target of a commercial car wheel, DP590 (5.6mm, ferrite + martensite) and FB540 (4.0 mm, ferrite + bainite) are used to manufacture wheel spoke and rim, respectively. They are used to replace the original 510L (6.6mm) and 380CL (4.8mm) steels. Stamping and bake paint are two essential steps in the fabrication of steel wheel, both of which will result in steel hardening [14], thus the variation of mechanical property of steel should be not ignored in further simulation. The average plastic strain in stamping is 0.02-0.05 mm/mm for car wheel, and 0.02 mm/mm pre-strain (plastic strain) is adopted as an approximation of strain hardenability in steel. The as-received steels (DP590r and FB540r), the steels with 0.02 mm/mm pre-strain (DP590rp and FB540rp) and also that with 0.02 mm/mm pre-strain and bake hardening (DP590rpb and FB540rpb) are used and compared in the experiment and numerical simulation of strain fatigue.

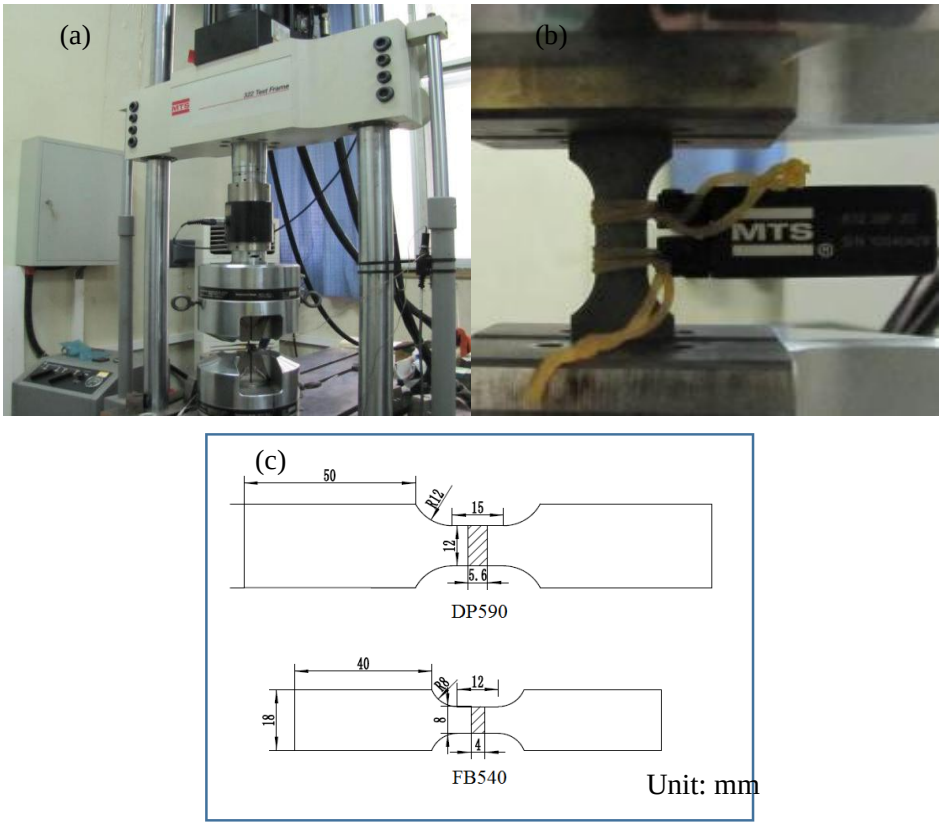

Fig.1. Details about Strain-fatigue experiment (a) MTS322 ±250kN hydraulic pressure servo testing machine, (b) extensometer, (c) flat specimen dimension in fatigue testing.

The specimen with 0.02 mm/mm pre-strain is processed as follows: the strain-stress curve of the specimen is obtained via tensile testing. A straight line with slope of elastic modulus is plotted starting from 0.02 mm/mm on X-axis. The intersection between the straight line and the engineering strain-stress curve is the final stop or destination to obtain 0.02 mm/mm pre-strain in the next tensile testing. The stress value of this intersection is selected to be the stopping signal because of its much larger magnitude than that of strain. Another specimen is pulled on the tension tester and stopped at the stress value mentioned above, and then specimen with 0.02 mm/mm pre-strain is achieved. In subsequent bake process, the specimens are baked at 170 °C for 30 minutes in a resistant furnace. The bake condition is completely consistent with the industrial paint process of automobile steel. The strain fatigue testing is performed on MTS322 ±250kN hydraulic pressure servo fatigue testing system. The cyclic strain ratio and frequency is -1 and 0.02-1.0 Hz, respectively. The

total strain amplitude $\Delta\varepsilon_t/2$ ranges from 0.003 mm/mm to 0.01 mm/mm in different experimental cases, and $\Delta\varepsilon_t/2$ is controlled via an extensometer. The fatigue system, extensometer and specimen dimension are illustrated in Fig.1 (a), Fig.1 (b) and Fig.1 (c), respectively. At each strain amplitude, stress-strain curve is obtained when hysteresis loop is stable after several tension-compression cycles.

2.2 Radial testing of car wheel

The specimen in radial testing is car wheel integrated with tire after bake paint, and the tester is a larger rolling drum. When the testing is performed, the rolling drum is driven by a bearing and then loads a pressure on the surface of tire, thus the wheel rotates continuously until final fracture takes place. The radial testing device is illustrated in Fig.2. The pressure loaded on tire is 22,510 N, and the least required fatigue life is 1,000,000 cycles for this wheel. Six wheels are tested in the experiment. The structure of the wheel is shown in Fig.3. According to GB/T 5334-2005 “Performance requirements and test methods of passenger car wheels”, the rapid decline of loading force is the criteria for estimating the fatigue life of automobile wheel. The experiment is regularly stopped after 100,000 cycles to be checked visible crack on the surface, which is regarded as crack initiation. Moreover, 3,000,000 cycles is the up-limit in this fatigue experiment regardless of the state of the testing wheel.

Fig.2. The radial fatigue tester of car wheel

Fig.3. The structure of the wheel

2.3 Microstructure characterization

The specimen is cut from crack location on the wheel after radial fatigue testing. Its microstructure is characterized by SEM. The morphology as well as the scheme of wheel fracture during radial fatigue testing is analyzed.

3. Simulation

3.1 Strain model of radial fatigue testing

Fatigue fracture is mainly induced by cyclic strain concentration at special location according to local stress-strain method, thus a strain model for simulating the rotation process of car wheel is essential. In this paper, the 3D elastoplastic finite element model is applied to simulate the strain distribution of car wheel in one circle during radial fatigue testing. Tetrahedral and hexahedral solid elements are applied in this model owing to the complicated geometry of wheel, in which the mesh size is about 6 mm. The integration of rim and spoke is accomplished via nodal joint. The mechanical parameters of DP590r+FB540r (Wheel 1), DP590rp+FB540rp (Wheel 2) and DP590rpb+FB540rpb (Wheel 3) are represented via cyclic strain-stress curves from fatigue testing. The wheel is a 5-division symmetrical structure, in order to consider the complicated stress loading during a cycle, 6 static loading cases along the circumference are applied in this model. The tire pressure is taken into account and is homogenously loaded on the surface of rim with a value of 0.4 MPa. The displacements of nodes located on the edge of bolt hole are constrained to 0. All the boundary conditions of this strain model are illustrated in Fig.4. In each case, the

loading force on the rim is calculated by [16, 17]:

$$F = F_0 \cos(\frac{\pi}{2}\frac{\theta}{\theta_0}) \tag{1}$$

where F_0 is maximum radial loading force, F_0=22,510 N. θ is loading angle (between yellow dash line and green solid lines in Fig.4), and θ_0 is angle at maximum load (between yellow dash line and blue solid line in Fig.4).

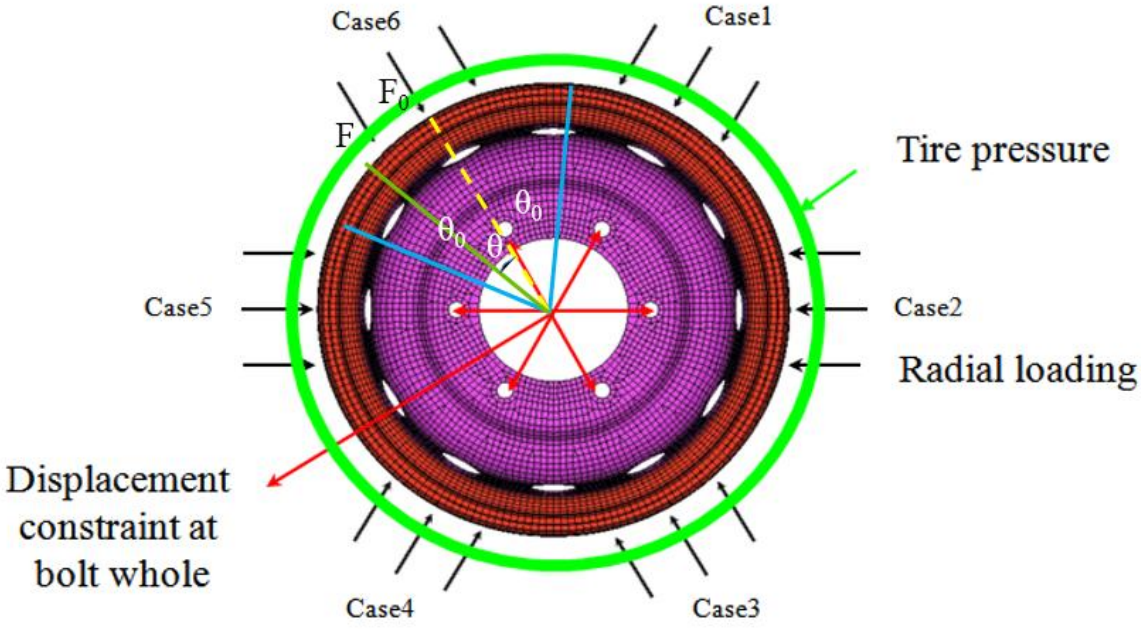

Fig.4. The loading cases in radial fatigue test. (Tire pressure is homogeneously loaded on the surface of wheel rim, while radial loading is located on the arc corresponding 60 ° central angel in each static loading case.)

3.2 Fatigue model of radial fatigue testing

The strain-life relationship can be represented by Manson-Coffin equation as follows:

$$\frac{\Delta\varepsilon_t}{2} = \frac{\Delta\varepsilon_e}{2} + \frac{\Delta\varepsilon_p}{2} = \frac{\sigma'_f}{E}\left(2N_f\right)^b + \varepsilon'_f\left(2N_f\right)^c \tag{2}$$

where $\Delta\varepsilon_t/2$, $\Delta\varepsilon_e/2$ and $\Delta\varepsilon_p/2$ are total strain amplitude, elastic strain amplitude and plastic strain amplitude, respectively, N_f is fatigue life, E is elastic modulus, σ'_f is

fatigue strength coefficient, b is fatigue strength exponent, ε'_f is fatigue ductility coefficient, and c is fatigue ductility exponent.

The Manson-Coffin model can predict the fatigue life of elastic or plastic deformed materials via corresponding strain amplitude. However, when fatigue life exceeds 10^5 cycles, the effect of surface and scale factors on the fatigue life of materials is significant, and they are involved to correct the elastic strain-based fatigue model. Thus the term of (σ'_f/E) in Eq.2 is corrected via the two factors, which is expressed via [18]:

$$(\frac{\sigma'_f}{E})' = \frac{\lg(\sigma_{-1}\mu\beta_1) - \lg(\sigma'_f - \sigma_m)}{\lg\sigma_{-1} - \lg(\sigma'_f - \sigma_m)}(\frac{\sigma'_f}{E}) \tag{3}$$

where σ_{-1} is fatigue limit, μ is scale parameter, β_1 is surface parameter, σ_m is mean stress. Here σ_{-1} is approximated as 0.5 times of the ultimate strength. $(\sigma'_f/E)'$ is actually the fatigue strength coefficient after the corrections of scale and surface factors, and the final values of $(\sigma'_f/E)'$ are listed in Table 1.

Table 1. Key parameters in Masson-Coffin model of various materials

Materials	σ'_f/E	$(\sigma'_f/E)'$	b	ε'_f	c
DP600r	0.0073	0.0083	-0.1373	0.05899	-0.3631
DP600rp	0.0057	0.0067	-0.1043	0.7230	-0.6689
DP600rpb	0.0053	0.0063	-0.1030	1.7887	-0.7885
FB540r	0.0021	0.0025	-0.05696	0.1982	-0.5522
FB540rp	0.0017	0.0021	-0.07838	0.0479	-0.6038
FB540rpb	0.0015	0.0018	-0.09743	0.3373	-0.5827

During the radial fatigue testing, the shape of air ventilation hole (just as a notch on specimen) has great effect on the stress concentration coefficient K_t [19], thus the size of air ventilation hole is applied to calculate the scale parameter, which is given as [6]:

$$\mu = \left(\frac{d_e}{7.62}\right)^{-0.1133} \tag{4}$$

where d_e is effective dimension, which is expressed via[20]:

$$d_e = 0.808(hd)^{0.5} \tag{5}$$

where *h* is average depth of the hole, h=5.6 mm, d is circumference of air ventilation hole, d=198.2 mm. Thus the scale parameter μ is 0.87 calculated by Eq. (4) and Eq. (5).The surface roughness of steel after hot rolling and pickling is about 1.2 μm. When tensile stress is about 650 MPa, the surface factor β_1 is 0.92 according to Ref. [19]. The strain simulation and fatigue prediction is carried out in ANSYS and its sub module Designlife, respectively.

4. Result and discussion

The mechanical properties of various steels are tested. The results are illustrated in Fig. 5. Fig. 5(a) shows the engineering strain-stress curves of DP590r, DP590rp and DP590rpb. It can be seen that the yield stress of DP590 steel is increased by 130 MPa after pre-strain and 200 MPa after pre-strain + bake, respectively. For DP590, it is more difficult to experience plastic deformation after being processed by pre-strain or pre-strain + bake. Fig. 5(b) shows that the mechanical property of FB540 steel is not sensitive to either pre-strain or bake especially near yield region.

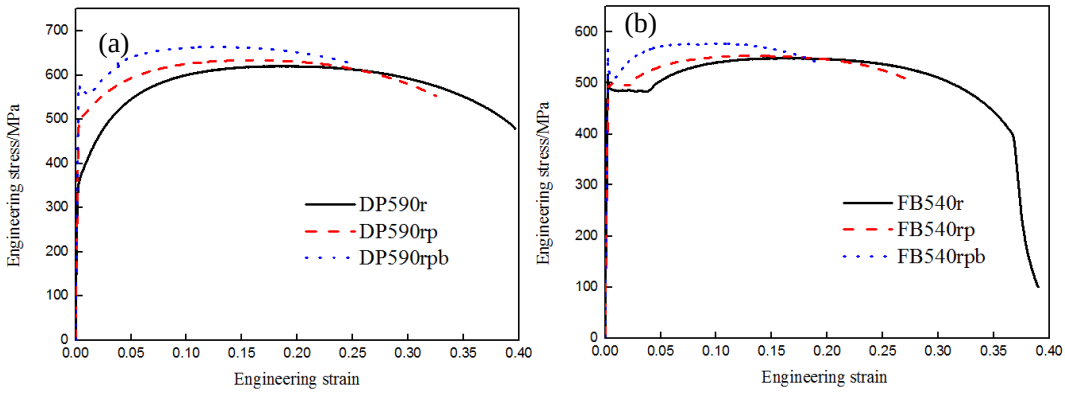

Fig.5. The Engineering stress-strain curves of steel after various manufacturing processes: (a) DP590, (b) FB540

Fig.6 presents the cyclic strain-stress curves of various materials. The plastic strain amplitudes under constant stress can be tested via extensometer, thus the cyclic strain-stress curves can be obtained via plotting experimental data. As seen in Fig.6 (a), in the strain range of 0-0.01 mm/mm, the effect of pre-strain and bake processes on strain-stress curve of DP590 still exists in cyclic tension-compression testing, after that the stress value tends to be the same. As the cyclic strain-stress curves of FB540

steel seen in Fig.6 (b), the cyclic mechanical property of FB540r is slightly decreased after pre-strain and bake hardening, in which the difference is very small. The cyclic strain-stress data will be further applied in the strain model to simulate the rotation process of car wheel.

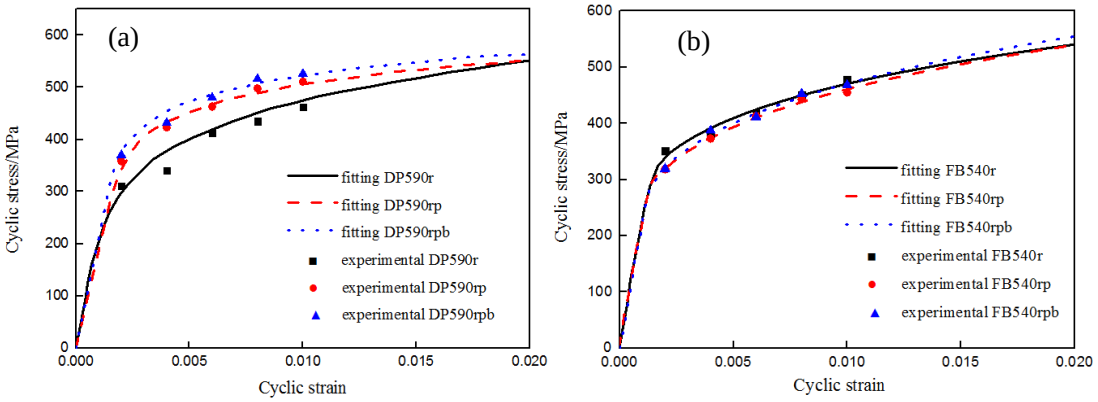

Fig.6. The cyclic stress-strain curves of steel after various manufacturing processes: (a) DP590, (b) FB540

The experimental data of fatigue life vs. elastic, plastic and total stain amplitudes as well as the fitting curves are plotted in Fig.7. The coefficients in Eq. (2) are obtained via these fitting curves and listed in Table 1. As shown in Fig.7 (a), (b), (c) and Table 1, the pre-strain and bake processes increase the fatigue life of DP590 steel when strain-fatigue curve are located in low fatigue life area (<1000 cycles). The effect of pre-strain on fatigue life is still controversial. Normally, fatigue life is governed by the ductility of a material at high strain amplitudes and by its strength at low strain amplitudes. S. Ganesh Sundara Raman [21] found that the fatigue life of 304 LN stainless steel with 30% pre-strain is smaller than that with 10% pre-strain at high strain amplitude. However, when pre-strain is much smaller, other people gave contrary findings. For example, Sperle [22] pointed out 2%, 4% and 8% tensile prestrains and subsequent bake hardening could improve fatigue resistance of DP steel. Robertson et al [23] reported that pre-strain and bake hardening could improve the fatigue life of TRIP steel at high strain amplitude, they attributed it to an increase of elastic-plastic ratio in this area. From a viewpoint of microstructure, plastic strain, high-density dislocations and micro-cracks mainly concentrate in ferrite during the deformation of DP590 steel, and then the dispersed martensite islands are promoted to

be integrated under the effect of flow ferrite. As a result, the accumulated martensite as well as high-density dislocations hinders the propagation of certain amount of micro-cracks in ferrite [24]. Perhaps the special microstructure containing very hard martensite and very soft ferrite in DP590 steel is the reason for its sensitivity of pre-strain and bake hardening. This is also why the effect of pre-strain and bake hardening on strain fatigue property is not so remarkable in FB540 steel as seen in Fig.7 (d), (c) and (f).

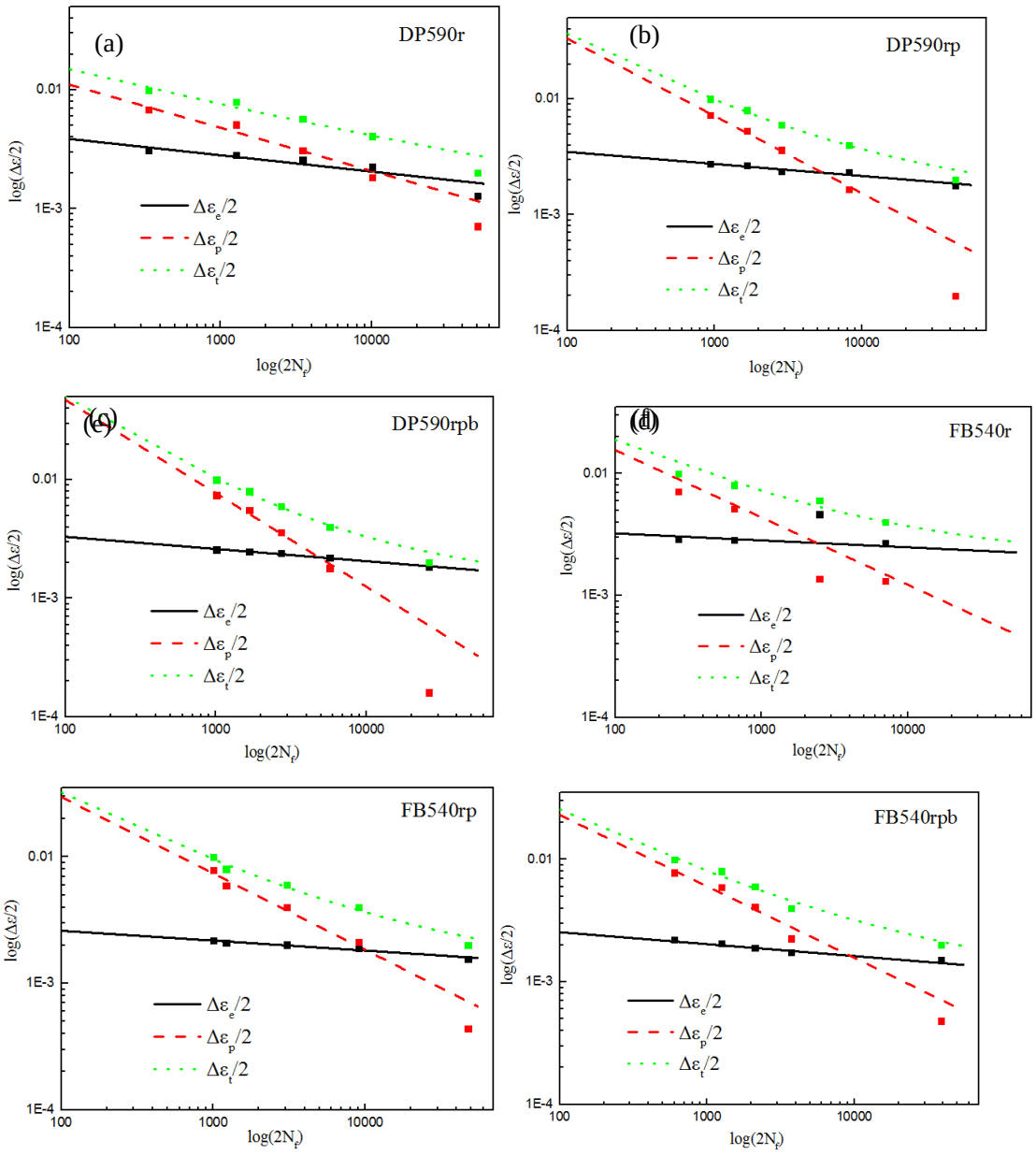

Fig.7. The strain-fatigue curves: (a) DP590r, (b) DP590rp, (c) DP590rpb, (d) FB540r, (e) FB540rp, (f) FB540rpb

The intersection of elastic and plastic lines appears at $2N_f$=10000 in DP590r. As a comparison, the location of intersection moves left in DP590rp, while the x-coordinate of intersection is the smallest in DP590rpb. This means it is easier to access plastic dominant area for DP590r than others, and is associated with increased crack initiation resistance and notch sensitivity [21]. In Fig.7 (d), (e), (f) and Table 1, the intersection moves right showing decreasing notch sensitivity after pre-strain and bake processes in FB540 steel, which corresponds to a slight loss of cyclic mechanical property.

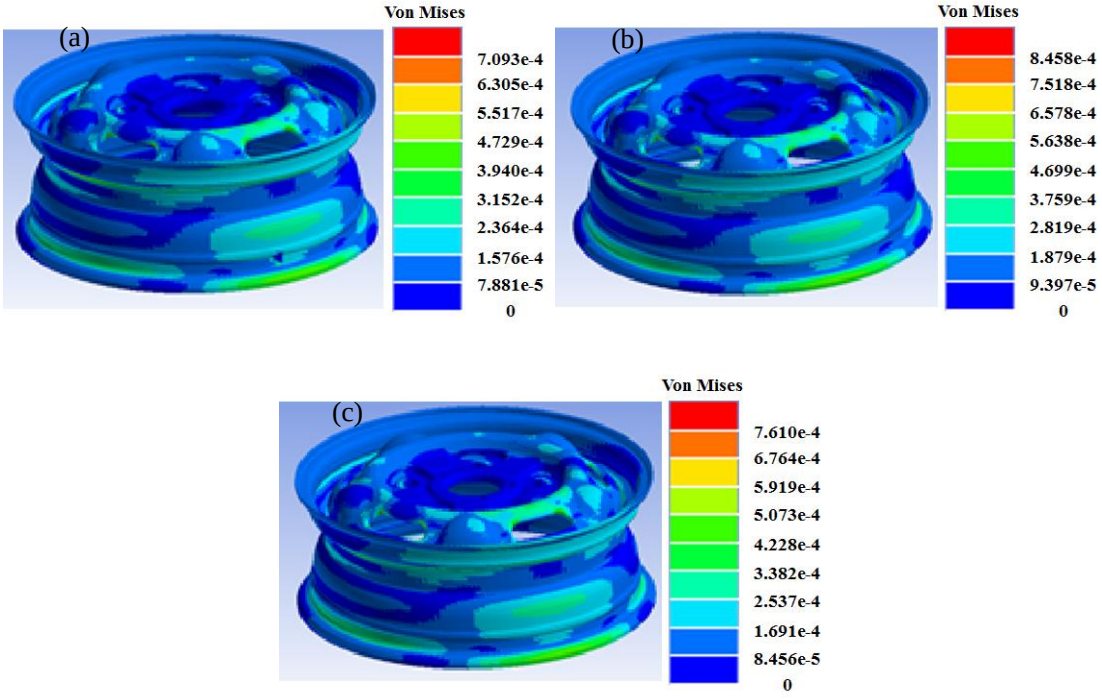

Fig.8. The strain distribution under radial fatigue test: (a) Wheel 1, (b) Wheel 2, (c) Wheel 3

The strain distributions for one static loading case of wheels are illustrated in Fig.8. The maximum strains of Wheel 1, Wheel 2 and Wheel 3 are 7.88×10^{-4} mm/mm, 9.40×10^{-4} mm/mm and 8.46×10^{-4} mm/mm, respectively. This indicates wheels only experience elastic deformation under the loads from radial fatigue testing. In each wheel, the peak strain locates at the corners of air ventilation hole. According to the results from mechanical testing, the elastic moduli of DP590r, DP590rp and DP590rpb are 212,491 MPa, 197,759 MPa and 209,395 MPa, respectively. This

means that the elastic modulus is decreased by pre-strain and subsequently slightly increased by bake hardening. The loss of elastic modulus of DP steel as the increase of plastic strain is also found in Ref [25-27]. It has been demonstrated that high-density dislocation resulted by plastic strain is the dominant factor of reduction in elastic modulus [28].The explanation from Mott [29] and Friedel [30] was the release of dislocations from locked or pinned sites (may be produced by plastic strain or other factors) would give extra elastic strain, which result in a decrease of elastic modulus. According to Hook's law, smallest elastic modulus corresponds to largest elastic strain when the same load is applied. This is why the peak value of strain in wheel 2 is the largest.

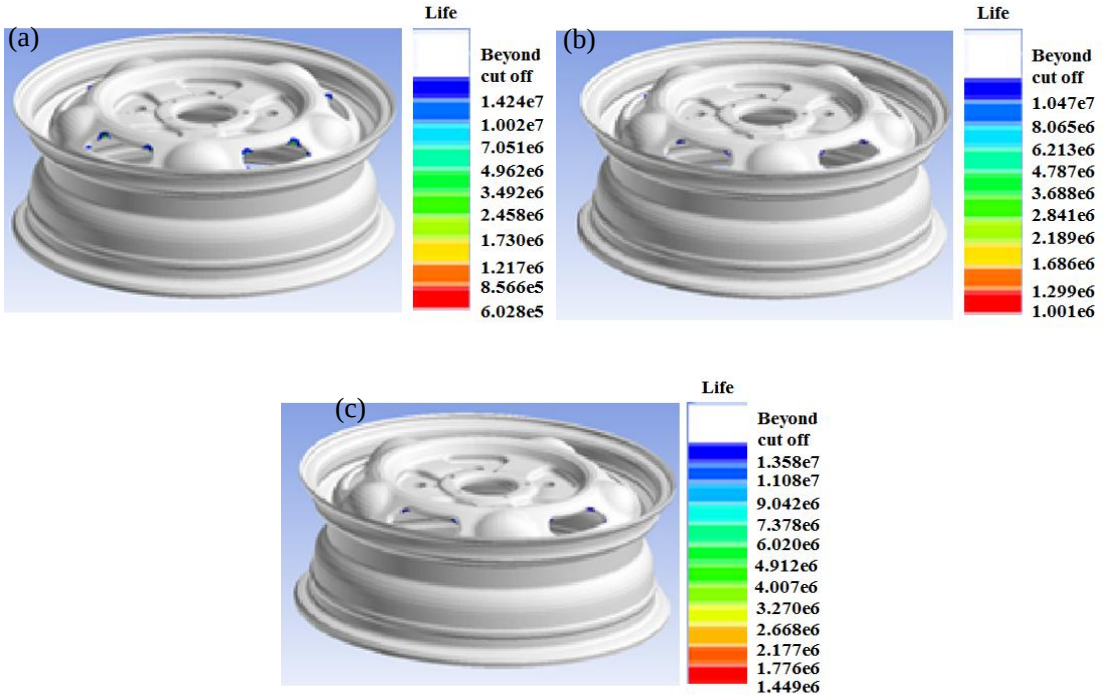

Fig.9. The fatigue life distribution under radial fatigue test: (a) Wheel 1, (b) Wheel 2, (c) Wheel 3.

Fig.9 shows the predicted fatigue life of wheel. It shows that cracks initiate at the corners of air ventilation hole, and the fatigue lives of Wheel 1, Wheel 2 and Wheel 3 are 602,000 cycles, 1,001,000 cycles and 1,449,000 cycles, respectively. The results indicate that the fabrication processes can effectively improve the fatigue property of wheel. The experimental results from radial fatigue testing are listed in Table 2. The simulation result is consistent with fatigue cycles at crack initiation but has certain

difference with the total fatigue life of wheel. The fatigue life of wheel is composed of crack initiation and propagation processes. The former is sensitive to fatigue property from specimen, scale and surface treatment factors, while the latter is mainly associated to obstacles from the microstructure of materials, such as grain size, slip system, dislocations, inclusion, defect, etc. If micro-obstacles display a high resistance of crack propagation, this process may take a large percent of the total fatigue life, i.e. the cracks slowly propagate and even finally stop under the defined loading. However, the parameters characterizing micro-obstacles and crack propagation mechanisms are not taken into account here, thus the present model has the limitation to predict the fatigue life of wheel when crack propagation take a large percent of the total process.

Table 2. The experimental results from radial fatigue tests of car wheel

Wheel	Cycles at crack initiation	Cycles at failure
Wheel 1	1,700,000	3,000,000
Wheel 2	1,700,000	2,826,884
Wheel 3	1,300,000	2,215,871
Wheel 4	1,500,000	2,398,329
Wheel 5	-	1,420,000
Wheel 6	1,200,000	1,533,422

Note: Visible cracks were not found on the surface of Wheel 5 before its failure.

Fig.10. Fracture morphology of wheel after radial fatigue test

Fig.10 gives the fatigue-failure wheel after radial fatigue testing. As shown in Fig.10, the crack initiates at a corner of air ventilation hole, and spreads along the

edge of air ventilation hole. The experimental result is consistent with the prediction of strain based fatigue model. Fig.11 illustrates the thickness measurement along the central line of wheel. The locations are marked in Fig. 11(a), and the thickness measurements of different locations are illustrated in Fig. 11(b). As shown in Fig. 11(b), the thickness of location 3 is reduced by 0.9 mm (thickness reduction is 16%), which also implies the strength at Location 3 is strongly increased by a larger plastic strain. According to Petrak's experimental results [31], steel with higher strength is more sensitive to crack propagation. It also can be seen in Fig.8, the strain concentration at Location 3 is more severe than those at other thinner locations (Location 8, 9, and 10). Meanwhile, Location 3 is adjacent to the corner of air ventilation hole (strain peak area). Probably, both strain concentration and crack propagation sensitivity at Location 3 induce the crack to propagate at this area.

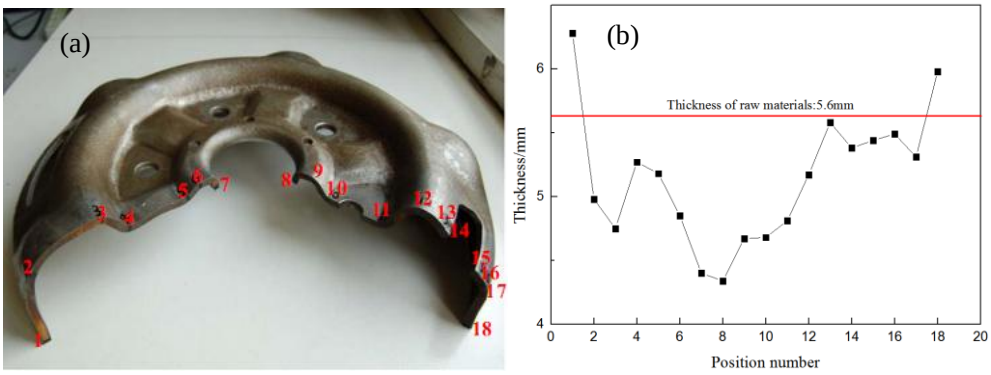

Fig.11. Thickness measurement along the central line of wheel

Fig.12 shows the fracture morphology near the crack. Fig. 12(a) indicates the macro morphology of sample including crack initiation (Area 1) and propagation (Area 2) zones. Fig. 12(b) illustrates the fracture morphology at Area 1. It can be seen from Fig. 12(b) that crack initiates from the surface of sample accompanied by some small dimples near the surface, then propagates inward with a quasi-cleavage pattern. The fatigue-induced crack initiation and propagation are mainly caused by cyclic slipping in the grains, thus fatigue fracture often displays a quasi-cleavage pattern rather than transcrystalline. Owing to a symmetrical tension-compression force, typical "fish bone" striations are formed in the area marked by red oval. Each striation is a record of micro plastic deformation in a cycle. From down to up in the red oval,

the size and space of striation trending to be larger indicate the increase of crack propagation rate. Fig.12(c) shows the morphology of fracture at Area 2. It is seen in Fig.12(c) that crack propagates in a pattern of quasi-cleavage fracture and is accompanied by arising secondary cracks.

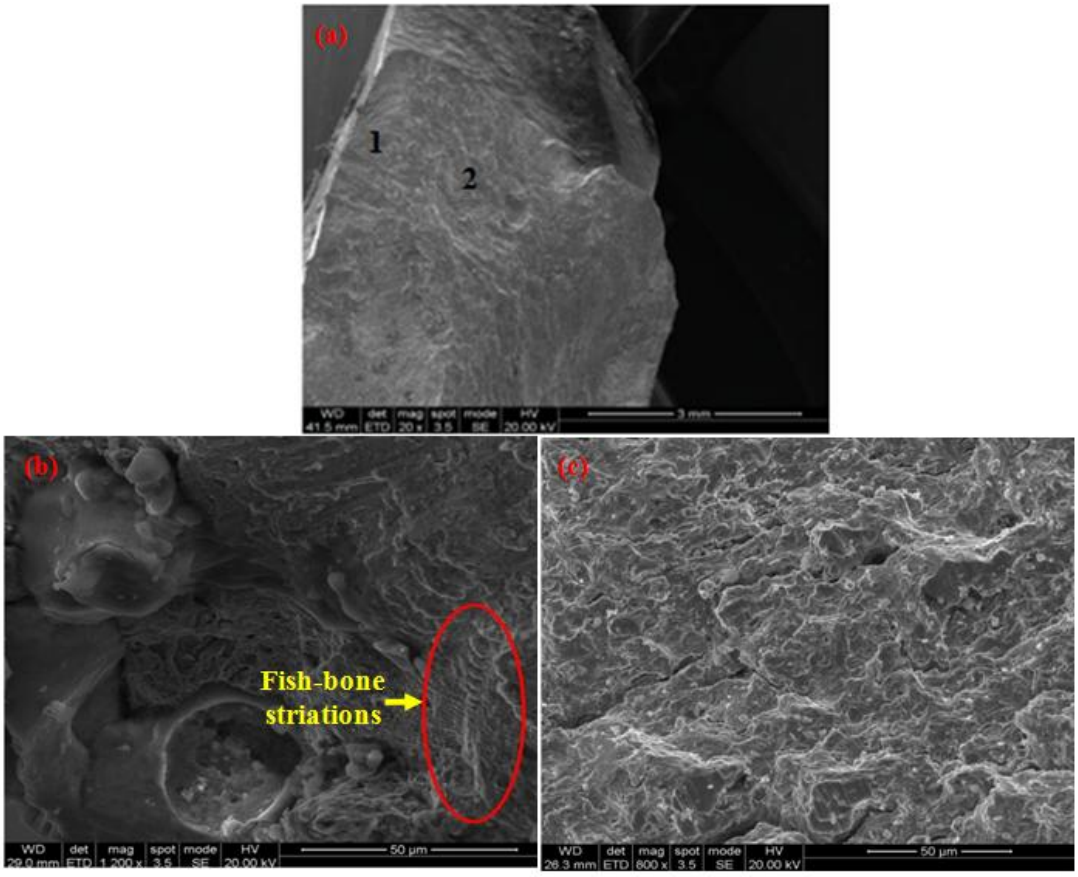

Fig.12 The SEM analysis of wheel fracture after radial fatigue test: (a) macro fracture morphology; (b) crack initiation area; (c) crack propagation area.

5. Conclusion

(1) The mechanical property of DP590 steel is sensitive to pre-strain and bake either in either monotonic tension or cyclic deformation, in which the yield stress is remarkably increased. However, the effect of both pre-strain and bake on the mechanical property of FB540steel is not remarkable. Moreover, the elastic modulus is reduced by pre-strain.

(2) The fatigue life of DP590 is improved by pre-strain and bake processes in high strain amplitude region, while the elastic-plastic transition is decreased. As a

comparison, these findings are not remarkable on FB540 steel.

(3) According to the strain simulation of wheel under radial loads, the peak strain occurs in Wheel 2, which is mainly because the deformations of all wheels are still in elastic state and the strain is determined by elastic modulus.

(4) The predicted fatigue life of Wheel 1, Wheel 2 and Wheel 3 is 602,000, 1,001,000 and 1,449,000, respectively. This means fabrication history can effectively improve the fatigue property of wheel. The simulation results are consistent with fatigue cycles at crack initiation in the experiments, but are limited to predict the total fatigue life when crack propagation accounts for a large portion.

(5) The SEM images show that, strain fatigue induced crack in DP590 steel initiates from the surface of sample accompanied by some small dimples, and then propagates in a quasi-cleavage pattern. “fish-bone” fatigue striations are found to show typical failure characteristics of strain fatigue.

Acknowledgement

The authors are grateful for the financial supports from National Natural Science Foundation of China (No.: U1564203), Chongqing Key Technological Innovation Special Program for Significant Industry (No.: cstc2015zdcy-ztzx50003), Chongqing Fundamental and Front Research Plan Outstanding Youth Project (No.: cstc2013jcyjjq60001).

Reference

[1] Meng J, Zhu P, Liu Z, Ji Q (2013). Integration of multi-step stamping effects in the bending fatigue analysis of a steel wheel. *Fatigue Fract. Engng. Mater. Struct*., 36, 795-808.

[2] Zheng Z, Sun T, Xu X, Pan S, Yuan S (2014). Numerical simulation of steel wheel dynamic cornering fatigue test. *Eng. Fail. Anal.*, 39,124-134.

[3] Raju PR, Satyanarayana B, Ramji K, Babu KS (2009). Evaluation of fatigue life of aluminum alloy wheels under bending loads. *Fatigue Fract. Engng. Mater. Struct*., 32, 119-126.

[4] Zhao Y, Ma M, Ling Y, Wang G, Fang G, Wan X (2016). A fatigue life model for

DP780 wheel during rotary bending process. Advanced High Strength Steel and Press Hardening: Proceedings of the 2nd International Conference (ICHSU2015), 359-364.

[5] Raju PR, Satyanarayana B, Ramji K, Babu KS(2007). Evaluation of fatigue life of aluminum alloy wheels under radial loads. *Eng. Fail. Anal.*, 14, 791-800.

[6] Topac MM, Ercan S, Kuralay NS (2012). Fatigue life prediction of a heavy vehicle steel wheel under radial loads by using finite element analysis. *Eng. Fail. Anal.,* 20, 67-79.

[7] Firat M, Kozan R, Ozsoy M, Mete OH (2009). Numerical modeling and simulation of wheel radial fatigue tests. *Eng. Fail. Anal.*,16, 1533-1541.

[8] Smith KN, Watson P, Topper TH (1970). A stress-strain function for the fatigue of materials. *J. Mater.*, 5, 767-778.

[9] Fatemi A, Socie DF (1988). A critical plane approach to multiaxial fatigue damage including out-of-phase loading. *Fatigue Fract Eng Mater Struct* .,11:149–165.

[10] Manson SS (1965). Fatigue: a complex subject – some simple approximations. *Expt. Mech.,* 5: 193–226.

[11] Coffin Jr LF (1954). A study of the effects of cyclic thermal stresses on a ductile metal. *Trans. ASME,* 76: 931–950.

[12] Wang X, Zhang X (2010). Simulation of dynamic cornering fatigue test of a steel passenger car wheel. *Int. J. Fatigue,* 32, 434-442.

[13] Neuber H 1961). Theory of stress concentration for shear-strained prismatic bodies with arbitrary nonlinear stress–strain law. *J Appl Mech, Trans ASME* , 24(4):544–550.

[14] Le Q, Kang HT, Kridli G, Khosrovaneh AK, Yan B (2009). Effect of prestrain paths on mechanical behavior of dual phase sheet steel. *Inter. J. Fatigue,* 31(4): 607-615.

[15] SHI M, Thomas GH, Chen MX, Fekete JR (2002). Formability performance comparison between dual phase and HSLA steels. *Iron & steelmaker*, 29(3):27-32.

[16] Stearns J, Srivatsan TS, Gao X, Lam PC (2006). Understanding the influence of pressure and radial loads on stress and displacement response of a rotating body: the automobile wheel. *Inter. J. Rotat. Machi.*

[17] Stearns J, Srivatsan TS, Prakash A, Lam PC (2004). Modeling the mechanical response of an aluminum alloy automotive rim. *Mater. Sci. Eng. A*, 366, 262-268.

[18] Zhao S (1997), *Design of fatigue resistance.* Mechanical Industry Press, Beijing, China.

[19] Schijve J (2009). *Fatigue of structures and materials, second edition*. Springer, Dordrecht, Holland.

[20] Shigley JE, Mischke C (1989). *Mechanical Engineering design*. MvGraw-Hill Inc, New York, USA.

[21] Ganesh Sundara Raman S, Padmanabhan KA (1996). Effect of prior cold work on the room temperature low-cycle fatigue behavior of ALSI 304LN stainless steel. *Int. J. Fatigue*, 18(2): 71-79.

[22] Sperle JO (1985). Fatigue strength of high strength dual-phase steel sheet. *Int. J. Fatigue*, 7(2), 79-86.

[23] Robertson LT, Hilditch TB, Hodgson PD (2008). The effect of prestrain and bake hardening on the low-cycle fatigue properties of TRIP steel. *Int. J. Fatigue*, 30, 587-594.

[24] Nakajima K, Urabe T, Hosoya Y, Kamiishi S, Miyata T, Takeda N (2001). Influence of microstructural morphology and prestraining on short fatigue crack propagation in dual-phase steels. *ISIJ Inter*., 41: 298-304.

[25] Andar MO, Kuwabara T, Yonemura S, Uenishi A (2010). Elastic–plastic and inelastic characteristics of high strength steel sheets under biaxial loading and unloading. *ISIJ inter.*, 50(4), 613-619.

[26] Chongthairungruang B, Uthaisangsuk V, Suranuntchai S, Jirathearanat S (2012). Experimental and numerical investigation of springback effect for advanced high strength dual phase steel. *Mater. Des.* 39, 318-328.

[27] Levy BS, Van Tyne CJ, Moon YH, Mikalsen C (2006). The effective unloading modulus for automotive sheet steels. *SAE Tech. Paper*, No. 2006-01-0146.

[28] Benito JA, Jorba J, Manero JM, Roca A (2005). Change of Young's modulus of cold-deformed pure iron in a tensile test. *Metal. Mater. Trans. A*, 36(12), 3317-3324.

[29] Mott NF (1952). CXVII. A theory of work-hardening of metal crystals. *Phil.*

Mag., 43(346), 1151-1178.

[30] Friedel J (1953). XLVI. Anomaly in the rigidity modulus of copper alloys for small concentrations. *Phil. Mag.*, 44(351), 444-448.

[31] Petrak GS (1974). Strength level effects on fatigue crack growth and retardation. *Engrg. Fracture Mech.*, 4: 725-733.